7th International Symposium on Three-Dimensional Electromagnetics
Vancouver, BC, Canada, November 13–15, 2023

FEMALY: A Finite Element MAtlab LibrarY for Electromagnetics

Klaus Spitzer[1], Jan Blechta[2,3], Jana Börner[1], Ralph-Uwe Börner[1], Michael Eiermann[4], Oliver Ernst[2], Mathias Scheunert[1]
[1]Institute of Geophysics and Geoinformatics, TU Bergakademie Freiberg, Germany
[2]Faculty of Mathematics, TU Chemnitz, Germany
[3]Mathematical Institute, Charles University, Prague, Czechia
[4]Institute for Numerical Mathematics and Optimisation, TU Bergakademie Freiberg, Germany

Summary

We present a finite element software library written in Matlab for the numerical simulation and inversion of electromagnetic fields in two and three dimensions. It is designed in a modular way to easily plug together fundamental building blocks for various electromagnetic applications from DC to the inductive range in the frequency and even time domain. External modules comprise the mesh generator and the equation solver library. Through its homogeneous software concept the adoption to any field application is relatively simple and makes the code suitable to open source distribution. We introduce the key features of this library including Lagrange and Nédélec finite elements formulated on unstructured tetrahedral grids, a Gauss-Newton inversion approach using linear Raviart-Thomas elements for H1 regularization, and the ability to incorporate any geometric feature such as topography, bathymetry and internal voids like caves, tunnels and mine buildings. The library is currently being tested with large real data sets to confirm its usefulness as a tool for practical data interpretation. Therefore, case studies for the magnetotelluric, direct current resistivity, controlled source electromagnetic and induced polarization methods in the field and laboratory are briefly outlined as examples with challenging geometric features.

Keywords: Finite elements, unstructured tetrahedral grids, Gauss-Newton inversion, regularization, Matlab

Introduction

The electromagnetics (EM) working group of the Freiberg Institute of Geophysics and Geoinformatics looks back on a long history of research in the field of simulation and inversion of geo-electromagnetic problems. Together with the Faculties of Mathematics of the Universities of Chemnitz and Freiberg, a wide variety of individual software solutions have been developed over the years. A collaborative software project over the last four years has enabled us to pool, unify, and re-implement the essential parts of the acquired knowledge into a single finite element (FE) software library written in Matlab, which is currently being tested and on its way to becoming an open source software for the EM community. After outlining the governing physics in terms of the underlying partial differential equations (PDE's) we present the key features of this library that allow for the implementation of the forward and inverse problem of any type of geophysical electromagnetic application in 2D and 3D ranging from the quasi-static to the inductive case in the frequency domain with arbitrary configuration of sources and receivers. Afterwards, we showcase successful applications in magnetotellurics (MT), direct current (DC) resistivity, controlled source electromagnetics (CSEM) and induced polarization (IP) as versatile examples with complex geometries.

The Forward Problems

The library provides solutions to the quasi-static EM case, typically the DC resistivity method, as well as passive and active induction methods in the diffusive domain.

For the quasi-static case, the equation of continuity for the scalar electric potential V in a domain Ω

$$\nabla \cdot (\sigma \nabla V) = -I\delta(\boldsymbol{x} - \boldsymbol{x}_0), \tag{1}$$

is solved for a point source of strength I and given electric conductivity σ. σ becomes complex-valued if IP effects are considered (Kemna, 2000).

In the diffusive induction case, a curl-curl-type of PDE in the frequency domain is considered using a time-harmonic e^{iwt} behavior (i imaginary unit, ω an-

gular frequency, t time) reading

$$\nabla \times (\mu^{-1} \nabla \times \boldsymbol{E}) - k\boldsymbol{E} = i\omega \boldsymbol{J}^S \tag{2}$$

where $k = i\omega(\sigma - i\omega\varepsilon)$ is the wavenumber, $\boldsymbol{E}$ the electric field, μ the magnetic permeability, ε the electric permittivity, and J^S some source term with the physical dimension of a current density. Appropriate boundary conditions have to be determined in each case. The FE method builds upon the transformation of the strong formulation of the boundary value problems (1) and (2) into the weak formulation of the problem with the identity only given in the sense of an inner product. To implement the approach we refer to the discrete formulation of the variational form which is achieved using the Galerkin approach that reduces the Ansatz function space $\mathcal{V}$ to a test function space $\mathcal{V}_h \in \mathcal{V}$ as the FE subspace of cellwise polynomial functions of order p over the spatial partition $\mathcal{T}_h$. This results in the reformulation of (1) and (2) as large linear systems of linear equations to be rapidly solved.

All solutions can be determined via optional total or secondary field approaches, the latter of which modify the right hand sides of eqs. (1) and (2) for the secondary sources with respect to a known background model. All material parameters can alternatively be selected as anisotropic. For further details, see Monk (2003), Schwarzbach et al. (2011), and Franke-Börner (2012).

The Inverse Problem

We have incorporated a standard regularized Gauss-Newton inversion approach minimizing a data objective functional Φ_d and a model objective functional Φ_m weighted by an unknown regularization parameter α reading

$$\begin{aligned}\Phi(\mathbf{m}) &= \Phi_d + \alpha\Phi_m = \\ \tfrac{1}{2}\|\mathbf{f}(\mathbf{m}) - \mathbf{d}\|_2^2 &+ \alpha||\mathbf{W}(\mathbf{m} - \mathbf{m}_{\text{ref}})||^2 \rightarrow \min_{\mathbf{m}}\end{aligned} \tag{3}$$

subject to $\mathbf{A}(\mathbf{m})\mathbf{u} = \mathbf{b}$. Here, $\mathbf{u}$ is the discrete solution vector (primary solution) of the PDE, $\mathbf{d}$ is the measured data, $\mathbf{f}(\mathbf{m}) = \mathbf{Q}\mathbf{A}(\mathbf{m})^{-1}\mathbf{b}$ the forward operator generating the modeled data, $\mathbf{m}$ the model parameter vector, $\mathbf{W}$ the parameter weighting matrix, $\mathbf{Q}$ the measurement operator extracting and transforming the solution at the observation locations ($\mathbf{Qu} \approx \mathbf{d}$), and $\mathbf{m}_{\text{ref}}$ is a reference model defining a preferred region of the model space. The linearized normal equations for an iterative process, i.e., for $\mathbf{m}_{k+1} = \mathbf{m}_k + \Delta\mathbf{m}$ then read

$$\begin{aligned}\left(\mathbf{J}^T(\mathbf{m}_k)\mathbf{J}(\mathbf{m}_k) + 2\alpha\mathbf{W}^T\mathbf{W}\right)\Delta\mathbf{m} = \\ \mathbf{J}^T(\mathbf{m}_k)[\mathbf{f}(\mathbf{m}_k) - \mathbf{d}] + 2\alpha\mathbf{W}^T\mathbf{W}(\mathbf{m}_{\text{ref}} - \mathbf{m}_k).\end{aligned} \tag{4}$$

with the Jacobian $\mathbf{J}(\mathbf{m}_k) = \frac{\partial \mathbf{f}(\mathbf{m})}{\partial \mathbf{m}_k}$. The weighting matrix $\mathbf{W}$ represents a regularization operator applicable to piecewise constant model parameters on unstructured grids and weak formulations. We have chosen to implement a smoothness regularization according to Schwarzbach & Haber (2013) in which the penalty function measures the norm of a weak gradient of the conductivity field using Raviart-Thomas elements of lowest order RT_0. This ensures the normal components between elements to be continuous. A discrete representation of the model objective functional then reads:

$$\Phi_m = (\mathbf{m} - \mathbf{m}_{\text{ref}})^T\mathbf{D}\mathbf{M}_{RT_0}^{-1}\mathbf{D}^T(\mathbf{m} - \mathbf{m}_{\text{ref}}) \rightarrow \min_{\mathbf{m}}. \tag{5}$$

with $\mathbf{W}^T\mathbf{W} = \mathbf{D}\mathbf{M}_{RT_0}^{-1}\mathbf{D}^T$, $\mathbf{M}_{RT_0}$ denoting the RT_0 mass matrix and $\mathbf{D}$ the discrete divergence operator. For more details, see Nocedal & Wright (2006); Weißflog (2016); Scheunert et al. (2016); Wang et al. (2018); Blechta & Ernst (2023).

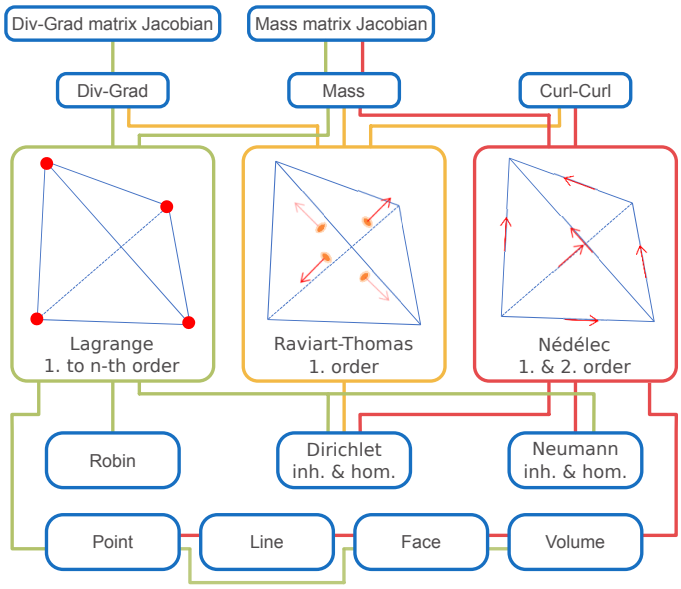

Figure 1: Building blocks for the forward modeling procedure: differential operator and their derivatives (top), types of FE (center), boundary conditions and source types (bottom).

The Code

The simulation and inversion code is entirely written in Matlab. It consists of FE forward modeling and

inversion building blocks and uses two external software packages: Gmsh (Geuzaine & Remacle, 2009) for the generation of unstructured tetrahedral meshes $\Omega = \bigcup_{\Omega_h \in \mathcal{T}_h} \Omega_h$ and MUMPS for the rapid solution of the resulting systems of linear equations (Amestoy et al., 2001). The following list gives an overview of the structure of the library.

- FE building blocks (see also Fig. 1)
  - Finite element definitions, i.e. basis functions of $\mathcal{V}_h$ with respect to $\mathcal{T}_h$:

    $V = \sum_i u_i \phi_i \quad \in H_h^1(\Omega) \quad \rightarrow$ Lagrange
    $\mathbf{E} = \sum_i u_i \boldsymbol{\psi}_i \quad \in H_h(\mathrm{curl}, \Omega) \quad \rightarrow$ Nédélec
    $\mathbf{p} = \sum_i u_i \boldsymbol{\chi}_i \quad \in H_h(\mathrm{div}, \Omega) \quad \rightarrow$ Raviart-Thomas
  - Bilinear forms, i.e. left-hand side, with respect to piecewise constant parameters $p = \sum_h p_h \Theta_h$ on Ω_h:

    $u_i \int_{\Omega_h} p_h \nabla \phi_i \cdot \nabla \phi_j \, \mathrm{d}V \quad \rightarrow$ Div-Grad
    $u_i \int_{\Omega_h} p_h \, \nabla \boldsymbol{\psi}_i \times \nabla \boldsymbol{\psi}_j \, \mathrm{d}V \quad \rightarrow$ Curl-Curl
    $u_i \int_{\Omega_h} p_h \, (.)_i \cdot (.)_j \, \mathrm{d}V \quad \rightarrow$ Mass
  - Linear forms, i.e. right-hand side, for continuous source functions:

    $\int_{\Omega_h} \delta(\boldsymbol{x}) \phi_i \, \mathrm{d}V \quad \rightarrow$ Point
    $\int_{\Gamma_h} f(\boldsymbol{x}) \boldsymbol{\psi}_i \cdot \boldsymbol{\tau} \, \mathrm{d}s \quad \rightarrow$ Line
    $\int_{\partial\Omega_h} \boldsymbol{f}(\boldsymbol{x}) \boldsymbol{\psi}_i \cdot \boldsymbol{n} \, \mathrm{d}A \quad \rightarrow$ Face
  - Jacobian, based on primary (.) and adjoint (.)′ solutions with respect to source s and receiver r and P^0 basis functions Θ_h:

    $\int_{\Omega_h} \Theta_h \nabla V_{i,s} \cdot \nabla V'_{j,r} \, \mathrm{d}V \quad \rightarrow$ Div-Grad Jacobian
    $\int_{\Omega_h} \Theta_h \boldsymbol{E}_{i,s} \cdot \boldsymbol{E}'_{j,r} \, \mathrm{d}V \quad \rightarrow$ Mass Jacobian

    (Lagrange, Nédélec)
- Boundary conditions
  - Dirichlet
  - Neumann (Lagrange, Nédélec)
  - Robin (Lagrange)
- Inversion building blocks
  - Scalable iterative solver (Blechta & Ernst, 2023) for H1-regularized normal equations
  - Gauss-Newton approach
  - Explicit Jacobian assembly
  - Line search (Armijo) (Nocedal & Wright, 2006)
- Gmsh mesh generation (Geuzaine & Remacle, 2009), DEM interpolation (Shepard, 1968) as shown in Fig. 2, VTK or XDMF export to Paraview (Ayachit, 2015)
- MUMPS parallel direct solver (Amestoy et al., 2001)
- Rational best approximation (Börner et al., 2008) for time integration

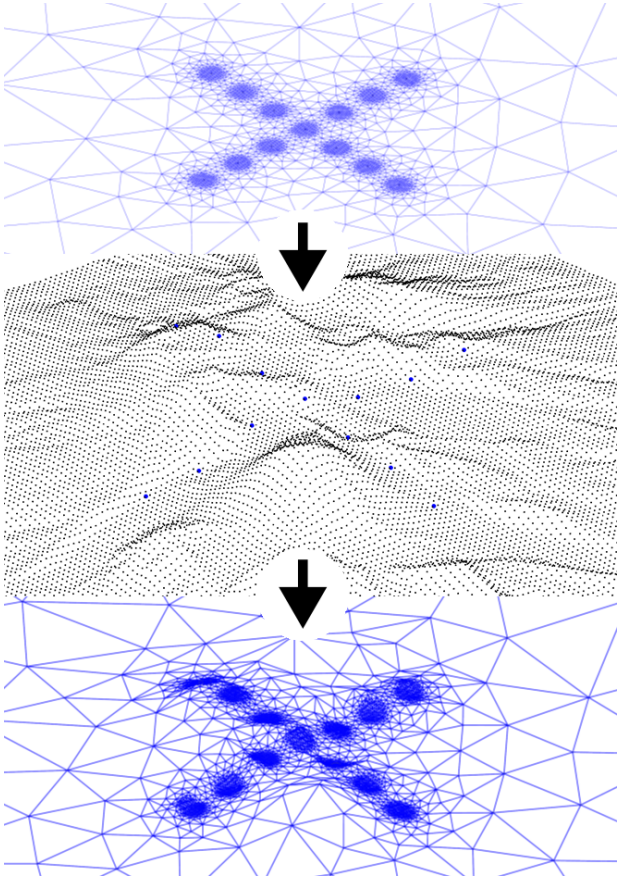

Figure 2: 2D surface with mesh refinement around sources/receivers (top), DEM with receiver locations shown as blue dots (center), 3D surface by adjusting mesh nodes using inverse distance weighting or C1 splines (bottom)

Applications

The following applications demonstrate the flexibility of the code and showcasing its successful performance for large, state-of-the-art field data sets collected in highly demanding geometric environments.

DC Resistivity in a Subsurface Mining Environment

The first example shows an in-mine DC resistivity survey in the 'Reiche Zeche', an educational ore mine

in the mining district of Freiberg, Germany (Fig. 3). The inner surface of the tunnel was scanned with a laser resulting in several hundred thousand geometry points being reduced to about 10000 points by triangulation. 80 electrodes were placed along the tunnel wall to conduct a Wenner-type survey cycling through the electrode positions with ten different spacings resulting in a total of 635 observations.

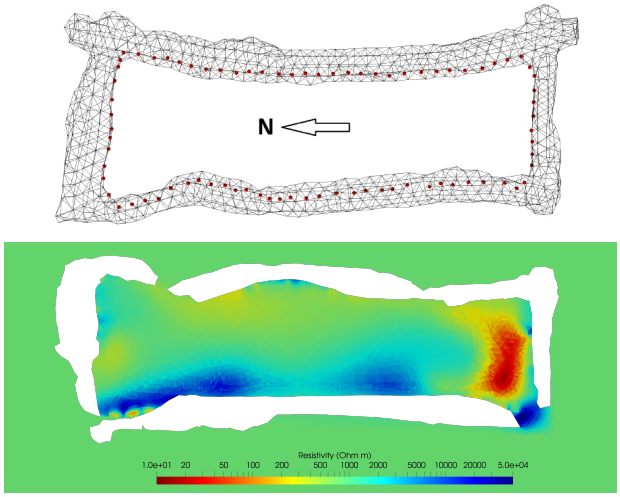

Figure 3: 3D Inversion of DC resistivity data collected in a subsurface mining gallery in Freiberg's 'Reiche Zeche'. Tunnel geometry with electrode locations (red dots, top) and inversion result (bottom). The shown tunnel system is approximately 35 m wide and 10 m high.

Magnetotellurics in Rugged Terrain

This section shows the inversion of a large MT data set from Mount Tarawera on New Zealand's North Island acquired by the Institute of Geological and Nuclear Sciences GNS (Bertrand et al., 2022). 68 MT sites were deployed over an area of 25 x 30 km^2 around the Tarawera Dome Complex between 2006 and 2017.

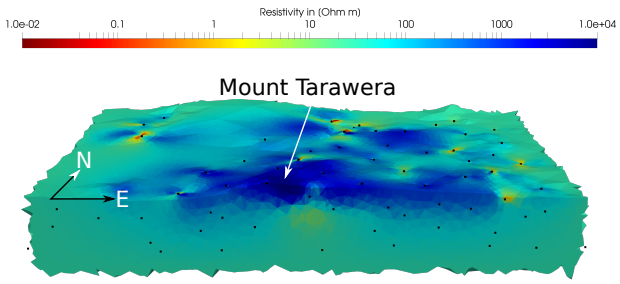

Figure 4: Preliminary inversion of a MT data set in the vicinity of Mount Tarawera, New Zealand.

For the 3D inversion, we have used 16 periods between 0.013 s and 341.297 s. Particular emphasis was put on an appropriate representation of the rugged topography. In a first attempt, we adapted the level of detailedness of the digital terrain model using an inverse distance weighting scheme. At the moment, we are working on a more elaborate sensitivity-guided refinement scheme because it became evident that some data were strongly affected by the terrain, particularly at sites less than 2 km away from steep slopes. Fig. 4 shows one of the inverted models.

Controlled-source Electromagnetics for Mine Monitoring

Based on surface-to-mine field campaigns at a large salt deposit we worked out the sensitivity footprint for the low-frequency (∼5 Hz to ∼300 Hz) CSEM sounding that uses large-scale line sources at the surface and oriented three-component magnetic sensors within the mine (Fig. 5). The mine is threatened by

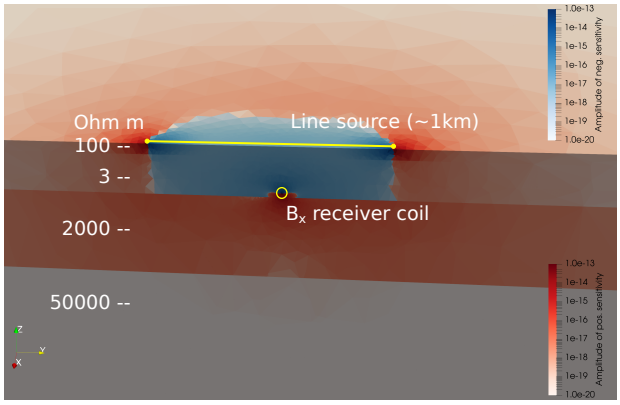

Figure 5: Sensitivity distribution (real part) for an exciting line source (∼40 Hz) on top of a layered halfspace for a surface-to-mine experiment in a Potash mine.

water intrusion dissolving the salt rapidly and creating large subsurface voids that lead to hazardous sinkholes at the Earth surface. To support the establishment of a monitoring system for the water infiltration into the mining galleries we carried out both, virtual experiments and sensitivity analyses for the surface-to-mine configuration as well as for a suggested mine-to-surface sounding with reversed source/receiver configurations. Moreover, first three-dimensional inversions were carried out with a preliminary data set (not shown here).

Induced Polarization in a Volcanic Environment

This application presents the inversion of IP data from a field survey at the rim of La Fossa crater on Vulcano Island, Italy. The multi-electrode data set, mainly dipole-dipole configuration, comprises 14 profiles of 14 electrodes each with 1 m spacing and 9 frequencies ranging from 91 mHz to 20 kHz. The domain model incorporates topography data from drone measurements. The obtained complex resistivity distributions in Fig. 6 highlight the fumarole-feeding hydrothermal system in the crater rim, revealed by consistently low resistivity and high phase shift.

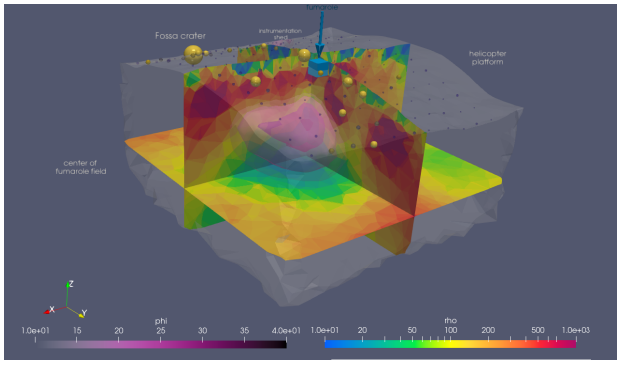

Figure 6: Resistivity and phase distribution beneath an active fumarole on the summit of La Fossa crater, Vulcano Island.

A Virtual Laboratory Experiment

The last application we present is a virtual accompaniment of a DC resistivity/IP laboratory experiment concerning the dynamic flow of electrically effective tracer fluids through a sample cylinder. Fig. 7 shows the geometry of the sample cylinder with current electrodes at the circular end faces and ring-shaped potential electrodes in narrow notches on the cylinder jacket. The conductivity distribution includes a spherical anomaly in the center part of the probe (top left). The top right-hand subplot shows the electric potential and the bottom left-hand subplot the current density. The sensitivity distribution shows the typical zones of positive and negative values (bottom right). Interestingly, the highest sensitivity values are reached at the contact line of the notches with the cylinder and not at the surface of the ring electrodes which is an important feature of the monitoring concept.

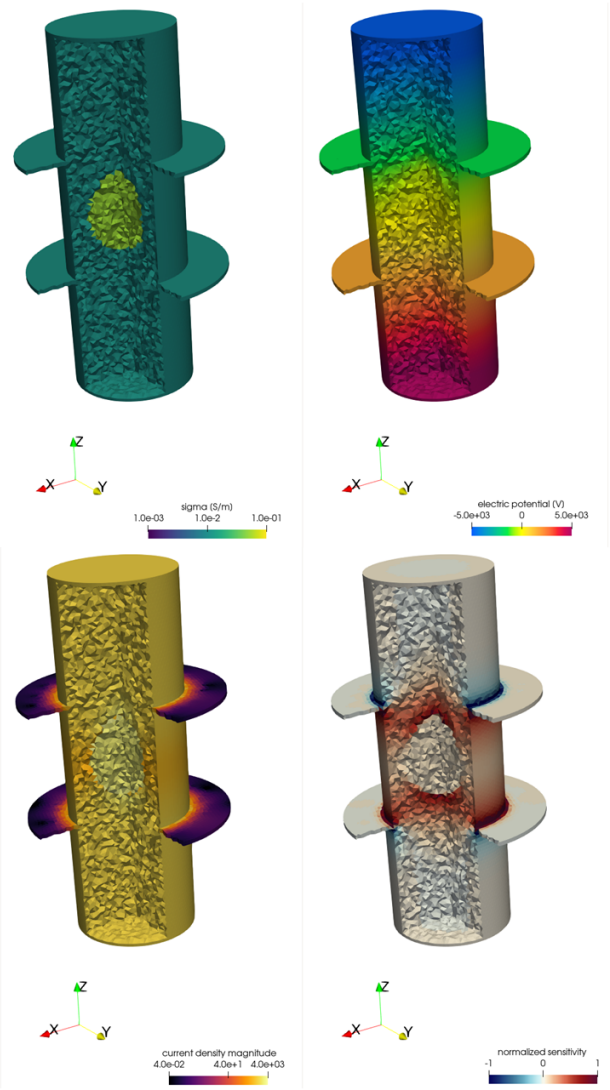

Figure 7: Laboratory cylindrical probe with current electrodes at the top and the bottom and two potential electrodes at the outer ring surfaces of disc-shaped bosses (top left: conductivity, top right: electric potential, bottom left: current density, bottom right: sensitivity).

Discussion and Conclusions

We have presented our finite element library for the simulation and inversion of electric/electromagnetic methods in geophysics and showcased some applications that we have worked on so far. The library is modular and homogeneously written in Matlab. It is planned to make the library available to the international community after our tests are completed.

The choice of the Matlab programming language has advantages and disadvantages. The advantages are a high-level programming language with the benefits

of an integrated development environment and convenient, straightforward, and math-oriented coding. Matlab has proven to be a long-term stable computing environment. However, the acquisition of a commercial license, which hinders the free exchange on a scientific level, can be seen as a disadvantage. Still, we believe that Matlab is widely available even in public and academic institutions and guarantees an enduring scientific software development.

All computationally intensive segments are processed through parallelizable external libraries. Visualization is done using Paraview. The interfaces are clearly defined, so that the external modules can be exchanged easily. Docker images may be provided in future for an uncomplicated setup and installation. Ready-made sample applications will be included which, as an easy starting point, can be adapted to individual new applications. We do hope that the present software development will be helpful to the community.

Acknowledgments

We thank the German Research Foundation (DFG) for continuous support over the years, the German Federal Ministry of Education and Research (BMBF) for funding within the GeoTechnologien Program, the EU for providing funding for the junior research group GeoSax within the European Social Funds (ESF) program, and all the collaborators and students who contributed.

REFERENCES

Amestoy, P. R., Duff, I. S., L'Excellent, J.-Y., & Koster, J. (2001). A fully asynchronous multifrontal solver using distributed dynamic scheduling. *SIAM Journal on Matrix Analysis and Applications*, *23*(1), 15-41.

Ayachit, U. (2015). *The paraview guide: A parallel visualization application*. Clifton Park, NY, USA: Kitware, Inc.

Bertrand, E., Kannberg, P., Caldwell, T., Heise, W., Constable, S., Scott, B., et al. (2022). Inferring the magmatic roots of volcano-geothermal systems in the rotorua caldera and okataina volcanic centre from magnetotelluric models. *Journal of Volcanology and Geothermal Research*, *431*, 107645.

Blechta, J., & Ernst, O. G. (2023). Efficient solution of parameter identification problems with h^1 regularization. *SIAM Journal on Scientific Computing*. (accepted for publication)

Börner, R.-U., Ernst, O. G., & Spitzer, K. (2008, 06). Fast 3-D simulation of transient electromagnetic fields by model reduction in the frequency domain using Krylov subspace projection. *Geophysical Journal International*, *173*(3), 766-780.

Franke-Börner, A. (2012). *Three-dimensional finite element simulation of magnetotelluric fields on unstructured grids on the efficient formulation of the boundary value problem*. Phd thesis, TU Bergakademie Freiberg, Freiberg, Germany.

Geuzaine, C., & Remacle, J.-F. (2009). Gmsh: A 3-D finite element mesh generator with built-in pre- and post-processing facilities. *International Journal for Numerical Methods in Engineering*, *79*(11), 1309-1331.

Kemna, A. (2000). *Tomographic inversion of complex resistivity*. Dissertation. Der andere Verlag. (Ruhr-Universität Bochum)

Monk, P. (2003). *Finite element methods for Maxwell's equations*. New York: Oxford University Press.

Nocedal, J., & Wright, S. (2006). *Numerical optimization*. New York: Springer Nature.

Scheunert, M., Ullmann, A., Afanasjew, M., Börner, R.-U., Siemon, B., & Spitzer, K. (2016). A cut-&-paste strategy for the 3-D inversion of helicopter-borne electromagnetic data — I. 3-D inversion using the explicit Jacobian and a tensor-based formulation. *Journal of Applied Geophysics*, *129*, 209-221.

Schwarzbach, C., Börner, R.-U., & Spitzer, K. (2011). Three-dimensional adaptive higher order finite element simulation for geo-electromagnetics-a marine CSEM example. *Geophysical Journal International*, *187*(1), 63-74.

Schwarzbach, C., & Haber, E. (2013). Finite element based inversion for time-harmonic electromagnetic problems. *Geophysical Journal International*, *193*(2), 615-634.

Shepard, D. (1968). A two-dimensional interpolation function for irregularly-spaced data. In *Proceedings of the 1968 23rd acm national conference* (p. 517–524). New York, NY, USA: Association for Computing Machinery.

Wang, F., Morten, J. P., & Spitzer, K. (2018). Anisotropic three-dimensional inversion of CSEM data using finite-element techniques on unstructured grids. *Geophysical Journal International*, *213*(2), 1056-1072.

Weißflog, J. (2016). *Three-dimensional individual and joint inversion of direct current resistivity and electromagnetic data*. Phd thesis, TU Bergakademie Freiberg, Freiberg, Germany.